# STRUCTURE VERSUS CHEMICAL FACTORS IN THE TRAPPING OF FLUOROQUINOLONE ANTIBIOTICS IN CLAY INTERLAYERS

A Thesis Presented to the Faculty of the Graduate School of Cornell University in Partial Fulfillment of the Requirements for the Degree of Masters of Engineering

by

Fanny Okaikue-Woodi

AUGUST 2016

Cornell University

Ithaca, NY

**ABSTRACT**

Many studies have been conducted on the adsorption of fluoroquinolone antibiotics (FQs) on Montmorillonite (MONT) and concluded that pH is the dominant factor in the interlayer adsorption of these FQs. However, little is known about how FQs of different generations adsorb onto MONT. In this study, we used both experimental and simulated data to further understand the interstratification of four different FQs, ciprofloxacin (CFX), ofloxacin (OFX), sarafloxacin (SFX) and moxifloxacin (MFX), at pH 5 and 7. The adsorption experiments show that adsorption was greater at pH 5 than pH 7. MFX showed higher affinity to MONT. X-ray diffraction analyses demonstrated that interlayer adsorption controls the extent of FQ adsorption. Molecular modeling reveals that the mechanisms of interactions that promote FQ trapping within the interlayer.

**ACKNOWLEDGMENTS**

I am grateful to Dr. Aristilde for the opportunity to work on this project, for her guidance and mentorship. I am thankful for the emotional and spiritual support of my friends and family. I express gratitude to Sabrina Kelch for her help with the X-ray diffraction analyses, and to all members of the Aristilde group for the memorable times we shared together.

## TABLE OF CONTENTS

## LIST OF FIGURES

## LIST OF TABLES

## Introduction

Fluoroquinolones (FQs) were initially developed in the 1980's based on the non-fluorinated fully synthetic antibiotic nalidixic acid (Figure 1A) [1] which was modified by the addition of a fluorine atom at position 6, a piperazine group at position 7 and the substitution of nitrogen atom at position 8 by a carbon atom (Figure 1B). The addition of the piperazine group improved the activity of FQs against Gram-negative species whereas the addition of the fluorine atom improved activity against Gram-positive species [1], thus making FQs broad spectrum antibiotics. Nalidixic acid is the prototypical first-generation quinolone antibiotics, which was subsequently followed by three generations of quinolones, all FQ antibiotics. Although the classification of FQs is arbitrary [2] and often based on their potency and microbial activity [1], there are some structural similarities among FQs of the same generation. The first generation of FQs, including compounds such as ciprofloxacin, ofloxacin, norfloxacin, enoxacin, directly resulted from the fluorination of nalidixic acid [3], and have a great antimicrobial activity against aerobic gram-positive bacteria but lacked activity against anaerobic bacteria [2]. Second-generation FQs have one (e.g. sarafloxacin) or two (e.g. fleroxacin) more fluorine atoms in their structure [3], and show greater potency against gram-negative bacteria [2]. Third-generation FQs, including moxifloxacin, gemifloxacin and trovafloxacin, are distinguished by structural modifications of the piperazine group and show greater potency against anaerobes and pneucocci [2].

These broad-spectrum antibiotics are widely used in human and veterinary medicine. Up to 90% of FQs consumed is not metabolized but excreted in the environment in concentration of ng $L^{-1}$ to ug $L^{-1}$ [4, 5], and have been detected in wastewater effluents [6,7,8], sewage sludge [9], sediments [10], surface waters [6,11,8], soils [12], and groundwater [6]. Additionally, the

application of manure and wastewater sewage sludge in agriculture results in increasing concentrations (2-450 ug $kg^{-1}$) of FQs in soils [4]. Soil pH and mineral content have been reported as important factors in the fate of FQs in soils and sediments [4]. In particular, the adsorption of FQs to clay minerals has been implicated in the retention of these antibiotics [4,13]. Of special interest is the mechanism of the retention of different types of FQ compounds within soil minerals.

Cation exchange, cation bridging, and hydrogen bonds have been suggested as possible mechanisms of interactions of FQs adsorption onto clay minerals, in particular smectite clays [14,15,16]. Smectite clays are 2:1 phyllosilicates clays of great importance to the fate of contaminants due to their swelling capacity that allows for the interlayer trapping of many antibiotics, their high specific surface area, and high cation exchange capacity [14, 17, 18]. As a result, adsorption of FQs have been reported to be higher in smectite-type clay minerals compared to non-swelling clays [13, 14, 15, 19, 20]. Smectite clays carry a negative permanent structural charge as a result of isomorphic substitutions in their interlayers [22]. This negative charge can be balanced by positively charged molecules. FQs bear a carboxylate and protonated amino groups resulting in their existence as cationic, zwitterionic and anionic species. A study on the adsorption of ciprofloxacin (CFX, Figure 2) on montmorillonite, illite and rectorite showed that there is a linear correlation between the amount of desorbed exchangeable cations and the amount of ciprofloxacin adsorbed at acidic pH (pH < 5.5) [19]. It was concluded, thus, that cation exchange is the major mechanism of adsorption of CFX onto clay minerals at acidic pH [19]. At acidic pH (pH $<pKa_1 = 6.7$), CFX exists in cationic form due to the protonated piperazine group and may replace exchangeable cations bound to the clay minerals [19, 21]. At high pH (pH 10-11), adsorption of FQs reportedly decreases [15, 16, 21] due to the repulsion

between the negatively charged clay minerals and anionic species of FQs [14, 16]. These studies imply that pH is a major factor in the adsorption of FQs to clay minerals.

Additionally, X-ray diffraction (XRD) analyses indicated the intercalation of FQ molecules within montmorillonite interlayers and revealed that FQ intercalation is also pH dependent [14, 21, 22]. Wang et al [18] reported an increase in the basal spacing ($d_{001}$) of Ca-montmorillonite as the amount of adsorbed CFX increases. The maximum $d_{001}$ was reached as the level of adsorbed CFX reached the maximum value obtained during isotherm experiments [16]. This positive relationship between montmorillonite basal spacing and adsorption capacities was also observed in the adsorption of enrofloxacin (ENR) [14], marbofloxacin (MAR) [14], and nalidixic acid on montmorillonite [13]. Another study [21] on the adsorption and intercalation of CFX on montmorillonite found that the expansion of the interlayer decreases as pH increases. In acidic pH, $d_{001}$ increased from 12.5 Å for raw montmorillonite to 18.3 Å for CFX-montmorillonite for an adsorption level of 298 mg $g^{-1}$ compared to an increase from 12.5 Å to 12.55 Å at alkaline pH for an adsorption level of 300 mg $g^{-1}$ [21]. This study confirms the pH dependence of the adsorption of FQs on montmorillonite. Additionally, it reported the existence of two $d_{001}$ peaks under circumneutral and basic pH and concluded that CFX intercalates differently under diverse pH.

Fourier transform infrared (FTIR) spectroscopy was performed in many studies to examine the mechanisms of interactions during FQs intercalation within clay interlayers [14, 21, 16, 19]. A shift (1385 $cm^{-1}$ to 1390 $cm^{-1}$) in the vibration band associated with the protonation of the amine group in the piperazine moiety was observed after adsorption of CFX onto montmorillonite, implying electrostatic interactions between the positively-charged piperazine moiety and the negatively-charged surface of montmorillonite [14, 16, 19]. In contrast, hydrogen

bonding was proposed as the mechanism of interaction between the carboxylate group and montmorillonite interlayer surface [14, 16, 19]. A shift in the ketone stretching band was explained by the release of intra-molecular hydrogen bonds between the keto group and the carboxylic group (Figure 2), to result in the hydrogen bonding of the carboxyl group and montmorillonite interlayer surface [14, 16, 19].

The aforementioned studies concluded that FQ intercalation within montmorillonite interlayers is pH dependent. Thus, all FQs would have the same adsorptive behavior. Figueroa-Diva et al. (2010) studied the trends in soil sorption coefficients ($K_d$) of three first-generation FQs: ciprofloxacin, enrofloxacin and norfloxacin [24]. They found that the $K_d$ values were the same for all three FQs on different soils. Thus, they concluded that adsorption of FQs was dependent only on their base structure (Figure 1C) without the influence of the different substituents. However, Rivagli et al (2014) hypothesized that the interactions with clay minerals may be structure-dependent because of the different substituents on the FQs' structures. [14]. In this study, we build on this hypothesis to elucidate the adsorption mechanisms of different generation FQs: ciprofloxacin (CFX, Figure 2), ofloxacin (OFX, Figure 3), sarafloxacin (SFX, Figure 4) and moxifloxacin (MFX, Figure 5). Additionally, previous studies lack a molecular characterization of the interstratification of FQs within montmorillonite interlayer. With XRD analyses coupled with molecular simulations, we aim to provide insights on the intercalation patterns of these FQs in order to better understand the differences in their adsorption behavior and interaction mechanisms.

A)

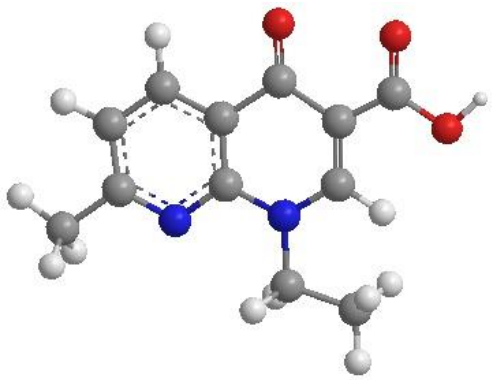

B)

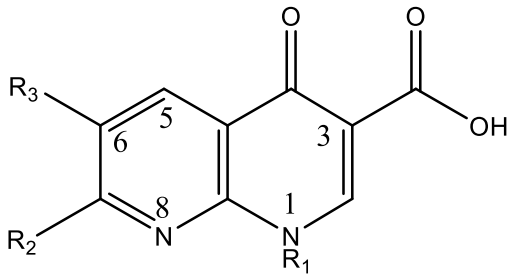


C)

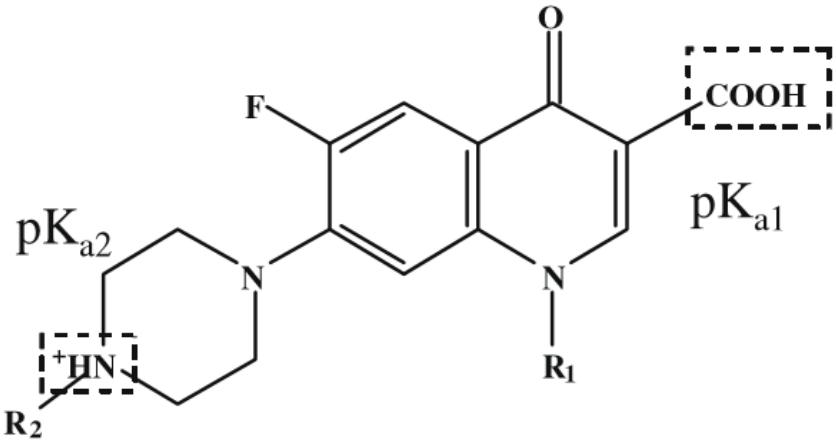


Figure 1. Molecular Structure of Nalidixic Acid (A), core nucleus of quinolone (B) and base structure of FQ (C)

**Materials and Methods**

*Materials*

Ciprofloxacin (CFX, molecular weight = 331.34 g $mol^{-1}$), ofloxacin (OFX, molecular weight = 361.37 g $mol^{-1}$), sarafloxacin hydrochloride (SFX, molecular weight = 421.83 g $mol^{-1}$) and moxifloxacin hydrochloride (MFX, molecular weight = 437.89 g $mol^{-1}$) were purchased from Sigma Aldrich. Figures 2-5 show the respective structures of these compounds along with their pH-dependent speciation. The pKa values for CFX, OFX, SFX, and MFX are respectively

6.1, 6.08, 6, and 6.1 for $pKa_1$ and 8.7, 8.25, 8.6 and 9.6 for $pKa_2$ [4, 25,26]. Montmorillonite (MONT) was obtained from the Clay Mineral Society and used as received.

The FQs concentrations in solution were measured with a Cary Eclipse Fluorescence Spectrophotometer from Agilent Technologies. Absorbance measurements were done with a Cary UV-Vis 60 from Agilent Technologies. The XRD analyses were done on a Bruker D8 Advance Powder X-ray Diffractometer with a Julabo HE-4 temperature control system and a Siemens ceramic X-Ray Tube.

A)

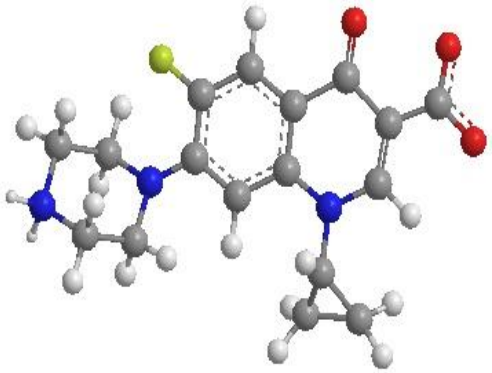

B)

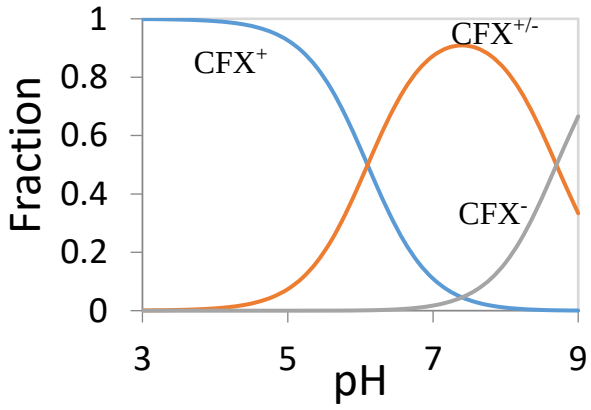


Figure 3. Molecular Structure of Ciprofloxacin (A) and its pH-dependent speciation (B)

A)

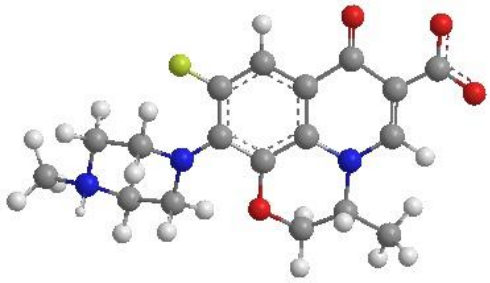

B)

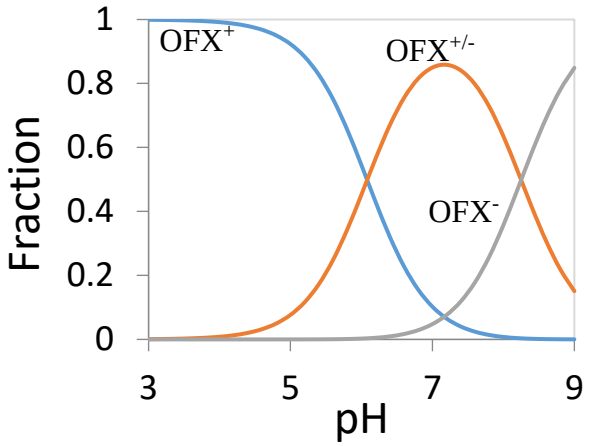


Figure 4. Molecular Structure of Ofloxacin (A) and its pH-dependent speciation (B)

A)

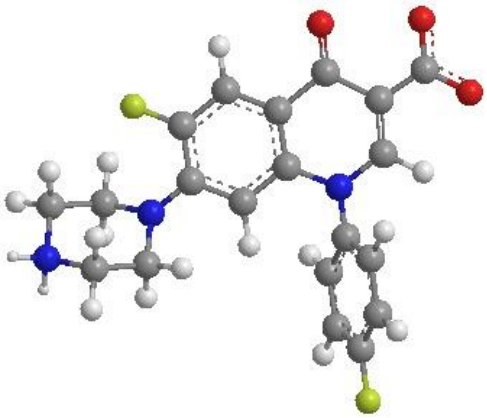

B)

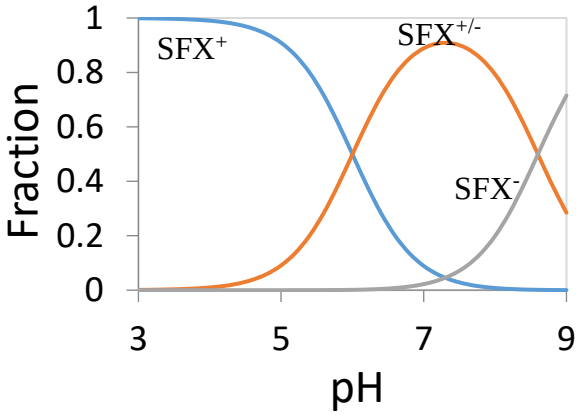


Figure 5. Molecular structure of Sarafloxacin (A) and its pH-dependent speciation (B)

A)

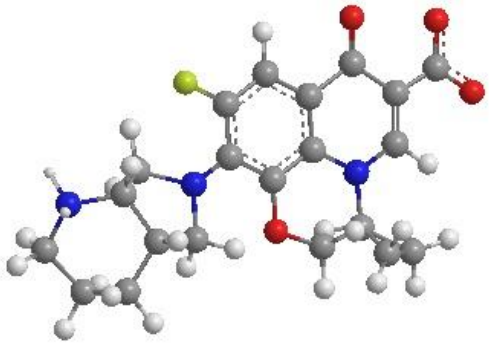

B)

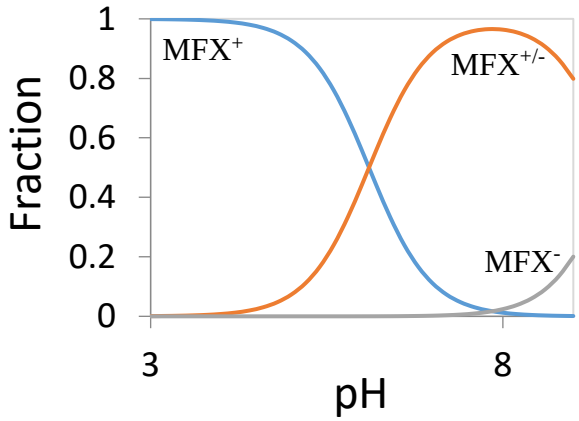


Figure 6. Molecular structure of Moxifloxacin (A) and its pH-dependent speciation (B)

Table 1. Speciation of the FQs compounds: Percentage of the different ionic species of the FQs at pH 5 and pH 7

| Compounds | pH 5 | | | pH 7 | | |
|---|---|---|---|---|---|---|
| | + | +/- | - | + | +/- | - |
| CFX | 92.6 | 7.4 | 0.0015 | 11 | 87.3 | 1.74 |
| OFX | 92.3 | 7.7 | 0.0043 | 10.2 | 85 | 4.78 |
| SFX | 90.9 | 9.1 | 0.0023 | 8.9 | 88.9 | 2.23 |
| MFX | 92.6 | 7.4 | 0.00018 | 11.2 | 88.6 | 0.22 |

*Adsorption and Kinetics Experiments*

The adsorption experiments were conducted by adding 40 mL of FQ solutions to 10 mg of Na-MONT in 50 mL tubes. Stock FQ solutions were prepared in 0.02 N NaOH to ensure complete dissolution of FQ compounds. Aliquots of the stock solutions were used to prepare the initial FQ concentrations of 25, 50, 75, 90, 100, 125 µM in a background solution of 1 mM $NaC_2H_3O_2$/$NaHCO_3$ and 10 mM NaCl adjusted to pH 5 and pH 7 with either 1 M NaOH or 1 M HCl. Table 1 shows the pH-dependent speciation of the FQs at pH 5 and 7. The tubes were covered in aluminum foil to prevent light-induced reactions. Reacted samples were centrifuged at 2000 *g* for 20 min and the supernatants were filtered with 0.2 µm filters. Kinetics experiments performed with initial concentration of 50 µM for all FQs at 4, 8, 12, and 24 h. At pH 5, CFX reached equilibrium at 12 h, MFX at 8 h, OFX and SFX at 4 h; and at pH 7, CFX, SFX, and MFX reached equilibrium at 4 h while OFX reached equilibrium at 12 h (Figure 6). The equilibrium adsorption experiments were conducted for 24 h. Adsorption experiments were done in triplicates whereas kinetics experiments were done in duplicates.

A)

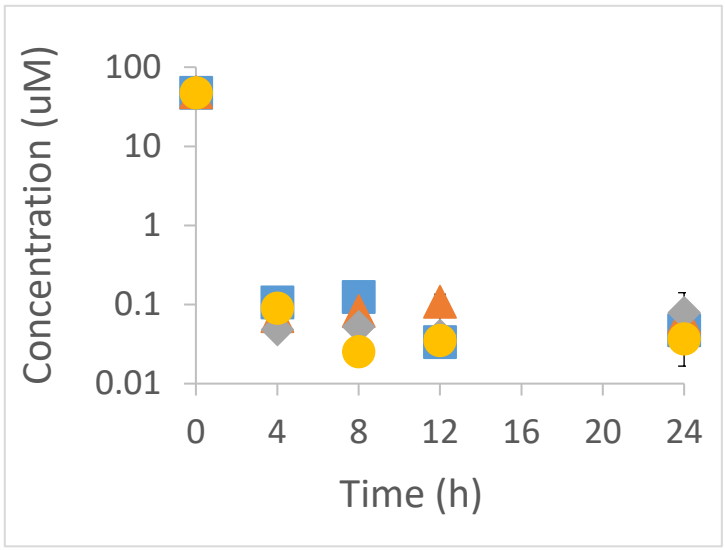


B)

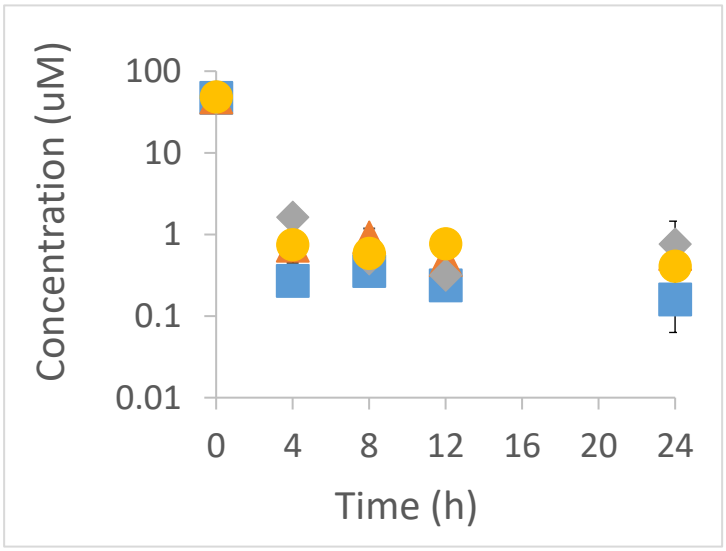


Figure 6. Kinetics of CFX ( ), OFX ( , SFX ( ) and MFX ( at A) pH 5 and B) pH 7

*Fluorescence Measurements*

Using a Cary Absorbance Spectrophotometer, the excitation peak wavelength of all FQs was initially detected (Table 2). Following a method by Aristilde & Sposito [27], full fluorescence spectra of all FQs were obtained at emission and excitation wavelengths from 400

nm to 600 nm and 250 nm to 350 nm, respectively, at 1 nm increments. The slit width was set to 2.5 nm and the scan rate was 10 nm $s^{-1}$. The peak excitation and emission wavelengths of each FQ are shown in Table 2 and Figures 7-10 show their full spectra. Fluorescence measurements were blank-corrected with the background solution and the concentration of FQ was calculated based on a calibration curve established with 5 standards in the case of each FQ and pH. The correlation coefficient $r^2$ was greater than 0.95 in all cases.

Table 2. Excitation and Emission Wavelengths

| Compounds | pH 5 | | pH 7 | |
|---|---|---|---|---|
| | Excitation Wavelength (nm) | Emission Wavelength (nm) | Excitation Wavelength (nm) | Emission Wavelength (nm) |
| CFX | 279 | 450 | 275 | 412.87 |
| OFX | 296 | 498.93 | 289 | 452.98 |
| SFX | 279 | 458.05 | 275 | 420.9 |
| MFX | 299 | 500 | 289 | 468.93 |

A)

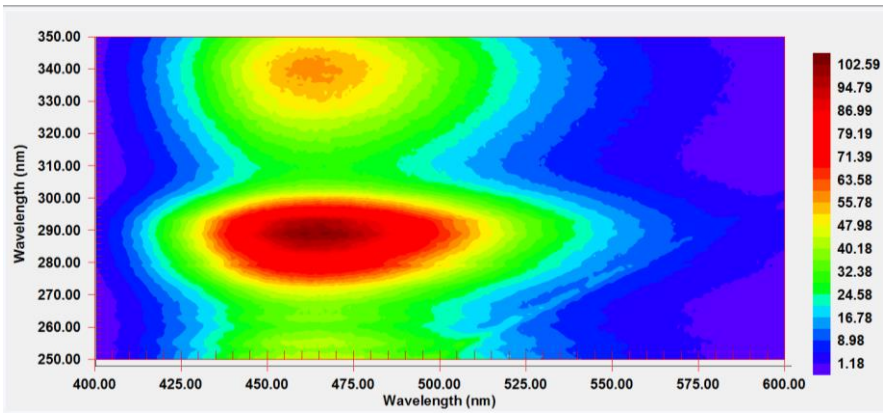

B)

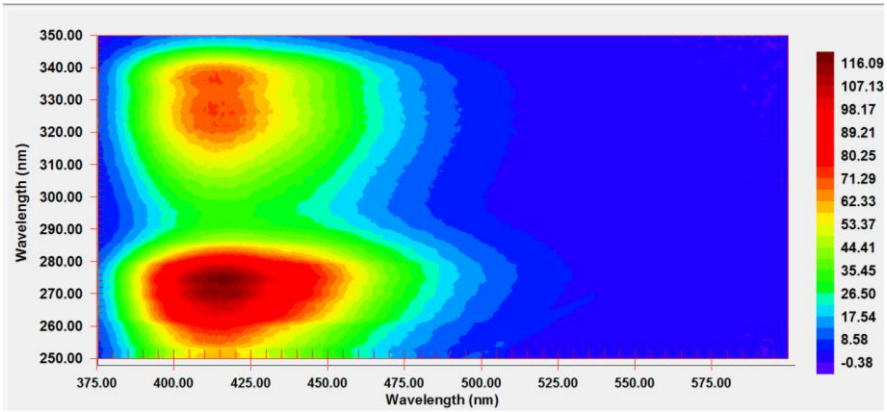


Figure 7. Fluorescence Spectra of CFX at A) pH5 and B) pH 7. Note that the emission axis was modified to show full spectra

A)

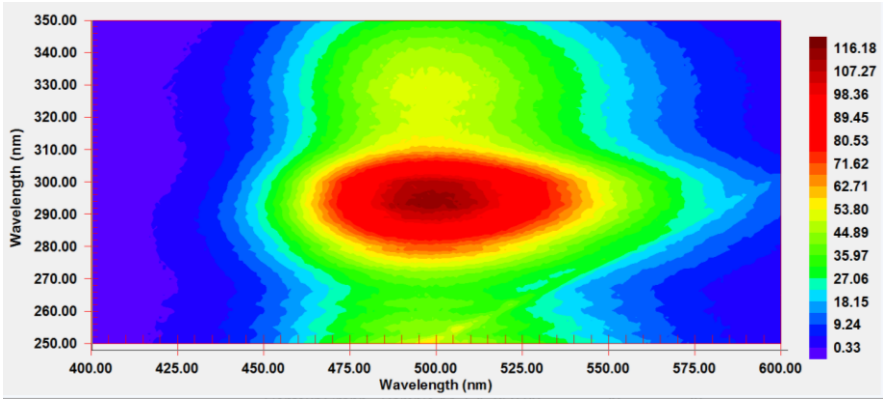


B)

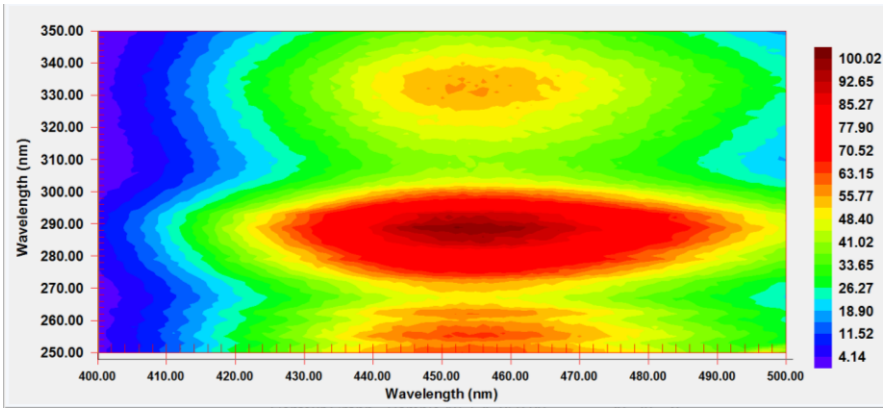


Figure 8. Fluorescence Spectra of OFX at A) pH5 and B) pH 7. Note that the emission axis was modified to show full spectra.

A)

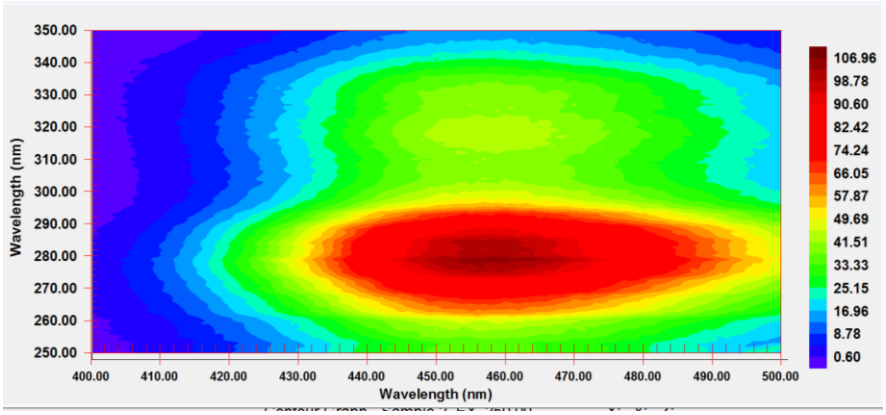


B)

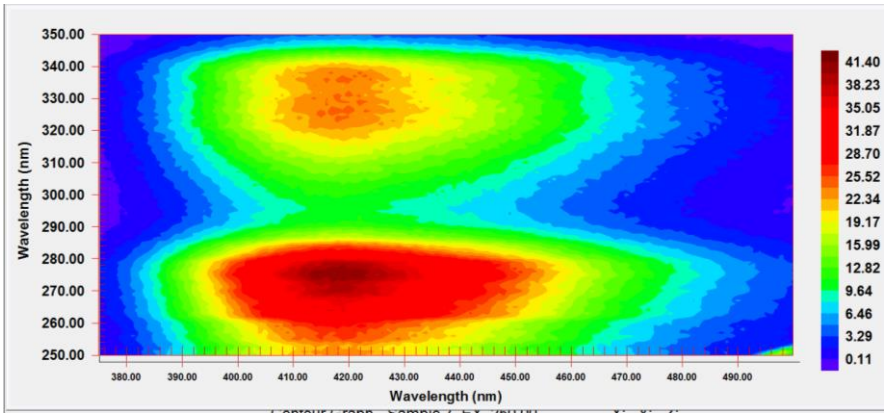


Figure 9. Fluorescence Spectra of SFX at A) pH5 and B) pH 7. Note that the emission axis was modified to show full spectra.

A)

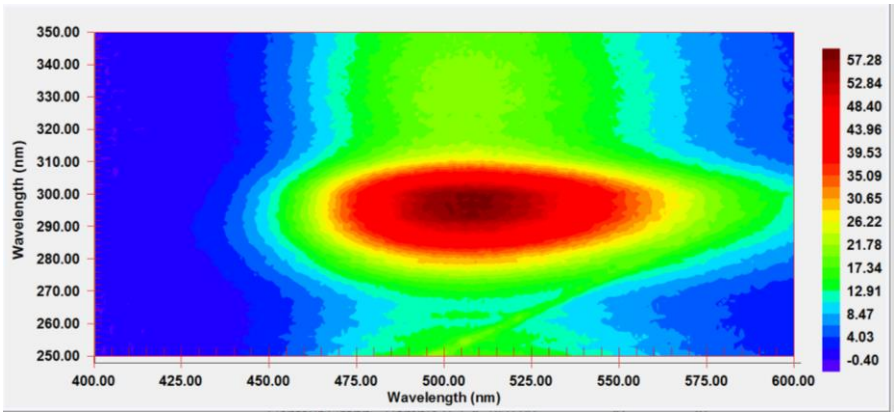

B)

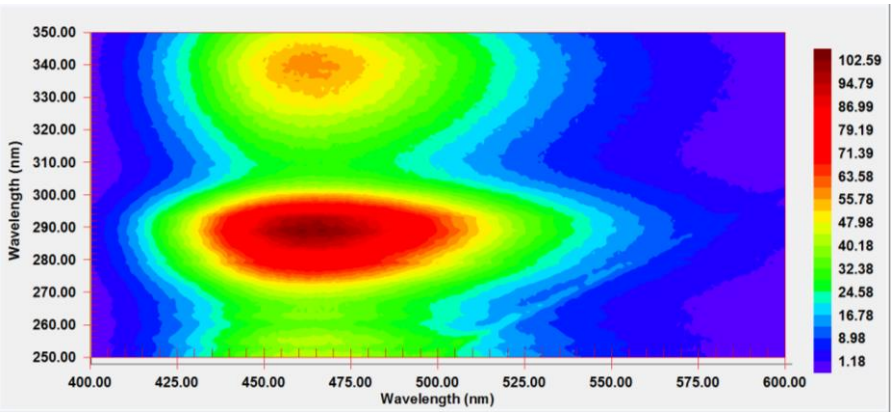


Figure 10. Fluorescence Spectra of MFX at A) pH5 and B) pH 7

*X-ray Diffraction Measurements*

The slurry samples at equilibrium were pipetted onto a flat sample holder then dried to a film for analysis. Measurements were taken at a constant temperature of 25 °C and relative humidity (RH) of 20 %. All XRD patterns were recorded with a Bruker D8 Advance Powder X-ray Diffractometer operated at 40 kV and 40 mA and equipped with an Anton Parr Eurotherm TCU110 temperature control unit and an Anton Paar CHC+ Cryo and Humidity Chamber in combination with a Prolumid MHG-32 Modular Humidity Generator. The scanning parameters were 0.02° 2θ step size and 8 s as counting time per step over the 1.5−8.5° 2θ Cu Kα angular range (λ = 1.5418 Å).

*Monte Carlo Simulations*

Monte Carlo Simulations were performed using the all-atom Condensed Phase Optimized Molecular Potentials for Atomistic Simulations Studies (COMPASS) forcefield included in the Material Studio software package [28]. The Adsorption Locator module of the software was used to conduct the annealing Monte Carlo simulations. A Wyoming-type model MONT with

(average) stoichiometry $Na_{0.5}(Si_8)$ $(Al_{3.5}Mg_{0.5})$ $O_{20}(OH)_{4,}$ unit cell of 2.112 x 1.828 x $d_{001}$ $nm^3$ and a total charge of -4 was used. The structures of CFX, OFX, SFX, and MFX zwitterions obtained through the ChemDraw software were validated to ensure that they could be simulated in the COMPASS forcefield. The partial charges for the water were initially assigned according to the extended simple point charge water model [29, 30], and the partial charges for the MONT according to the CLAYFF model [29, 31]. $Na^+$ ions at 10 mM ionic strength were used to counterbalance the negative charge of the clay. The adsorption of the four FQs were simulated respectively at 1.4, 1.6, and 1.8 nm in accordance to the XRD results. The number of water molecules at a constant density of 1 kg $dm^{-3}$ to be added in each interlayer was deduced by calculating the difference between the interlayer accessible volume and the Connolly volume of the FQs and counterions.

## Results

### *pH-Dependent Adsorption*

The adsorption isotherms of the four FQs at different pH are shown in Figures 11-14. Our analysis only included equilibrium concentrations ($C_e$) up to 10 μM in order to focus on concentrations found in environmental matrices [4]. For each FQ, adsorption was higher at pH 5 for increasing FQ equilibrium concentration greater or equal to 0.1 μM (Figures 11-14). The equilibrium concentrations were greater at pH 7 but the adsorption values (Q) were greater at pH 5 (Figures 11-14). For CFX, $C_e$ at pH 7 was 3.03 ± 0.28 μM and at pH 5, 2.52 ± 0.66 μM. For OFX, $C_e$ was 7.31 ± 0.41μM at pH 7 and 0.88 ± 0.21 μM at pH 5. For SFX, $C_e$ was 5.20 ± 0.38 μM at pH 7 and 3.69 ± 1.22 μM μM at pH 5. For MFX, $C_e$ was 1.6 ± 0.3 μM at pH 7 an 0.30 ± 0.0.1 μM at pH 5.

*Structure-Dependent Adsorption*

Figures 15 and 16 show the adsorption isotherms of the FQs on MONT at pH 5 and pH 7 respectively. At pH 5, all FQs have similar Q values, but Figure 15 show that their equilibrium concentrations were different. At pH 5, CFX has a Q value of 433.7 ± 48.6 μmol $g^{-1}$ and $C_e$ of 2.52 ± 0.66 μM. OFX has a Q value of 381.7 ± 0.8 μmol $g^{-1}$ and $C_e$ of 0.88 ± 0.21 μM. SFX has a Q value of 467.3 ± 1.2 μmol $g^{-1}$ and $C_e$ of 3.69 ± 1.22 μM. MFX has Q value of 433.7 ± 48.6 μmol $g^{-1}$ and $C_e$ of 0.30 ± 0.0.1μM. At pH 7, MFX has greater maximum Q values, but still has smaller $C_e$ values (Figure 16).

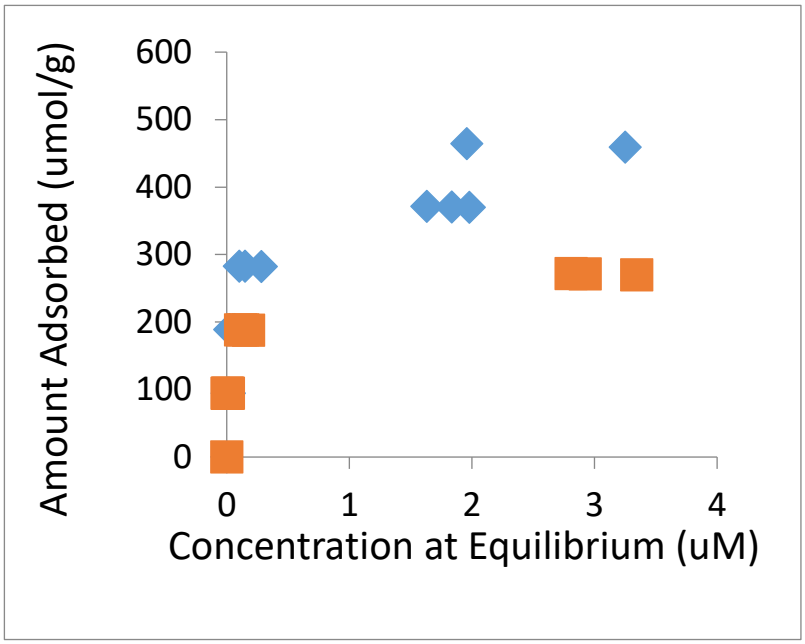


Figure 11. Adsorption Isotherm of CFX at pH 5 (◆) and pH 7 ( ■)

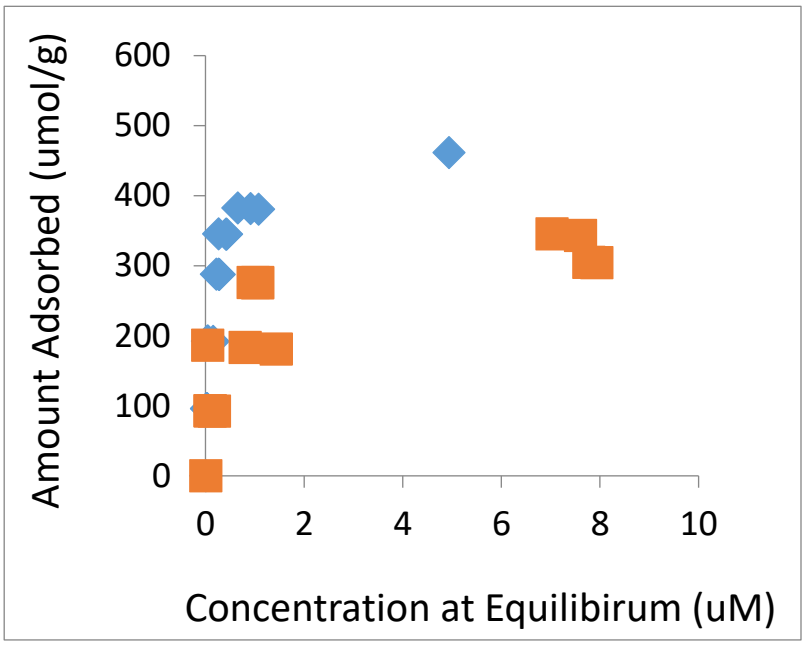


Figure 12. Adsorption Isotherm of OFX at pH 5 (◆) and pH 7 (■)

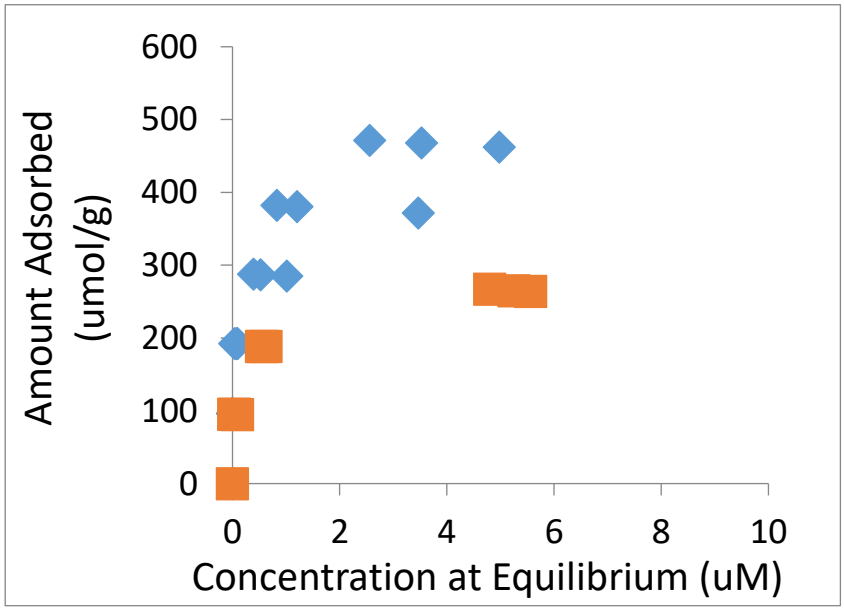


Figure 13. Adsorption Isotherm of SFX at pH 5 (◆) and pH 7 (■)

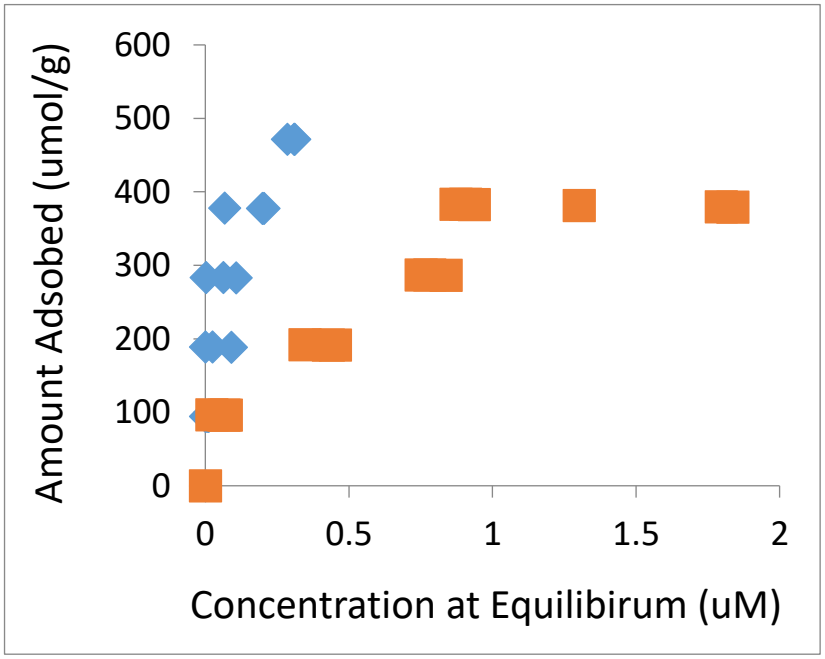


Figure 14. Adsorption Isotherm of MFX at pH 5 ( ) and pH 7 ( )

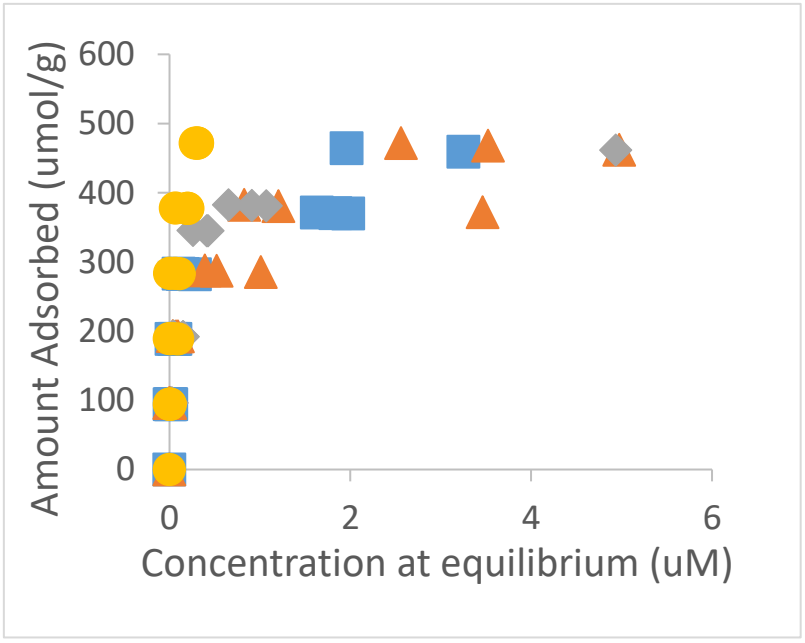


Figure 15. Adsorption Isotherms of CFX ( ), OFX ( ), SFX ( ) and MFX ( ) at pH 5

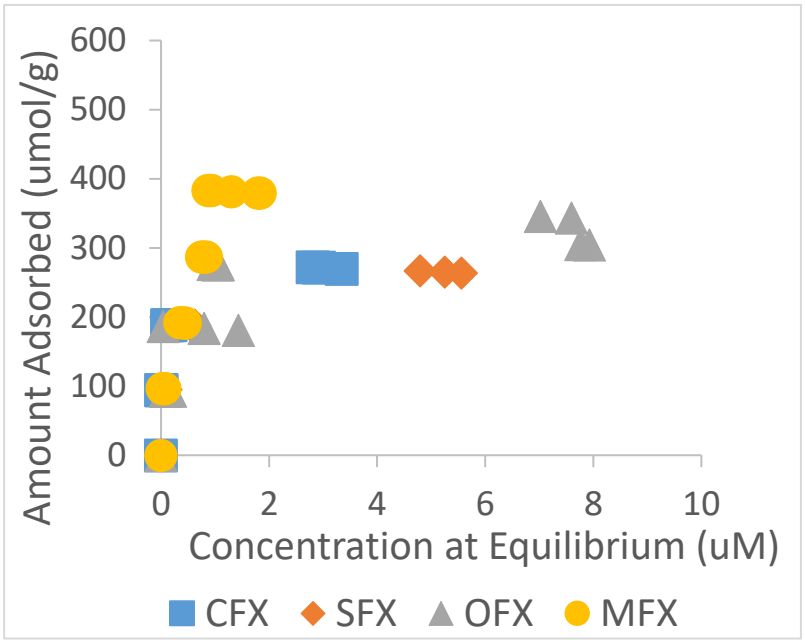


Figure 16. Adsorption Isotherms of CFX (■), OFX (◆), SFX (▲) and MFX (●) at pH 7

*Adsorption and Interstratification*

XRD Analyses

The basal spacing ($d_{001}$) was extracted from the XRD results and plotted against the adsorption equilibrium (Q) for each FQs at the respective pH (Figures 17-20). The $d_{001}$ for the pure clay was 0.998 nm at pH 5 and 1 nm at pH 7. In general, there is a positive relationship between $d_{001}$ and Q for all FQs; as Q increases, $d_{001}$ increases (Figures 17-20). At the same Q values, $d_{001}$ values were similar regardless of pH (Figures 17-20). For CFX, at Q value of 188.8 μmol $g^{-1}$, $d_{001}$ is 1.30 nm at pH 5 whereas for Q value of 188.1 μmol $g^{-1}$ at pH 7, $d_{001}$ is 1.31 nm (Tables 3-4). For OFX, at Q value of 287.9 μmol $g^{-1}$, $d_{001}$ is 1.40 nm at pH 5 whereas for Q value of 276.1 μmol $g^{-1}$ at pH 7, $d_{001}$ is 1.40 nm (Tables 3-4). For SFX, at Q value of 96.4 μmol $g^{-1}$, $d_{001}$ is 1.33 nm at pH 5 whereas for Q value of 95.1 μmol $g^{-1}$ at pH 7, $d_{001}$ is 1.32 nm (Tables 3-4).

Likewise, for MFX, at Q value of 189.1 µmol $g^{-1}$, $d_{001}$ is 1.42 nm at pH 5 whereas for Q value of 191.6 µmol $g^{-1}$ at pH 7, $d_{001}$ is 1.42 nm (Tables 3-4). Figures 21-22 compares the $d_{001}$ resulting from the intercalation of each FQ at both pH 5 and 7. At both pH, $d_{001}$ expansion was higher in the case of MFX intercalation. At pH 5, $d_{001}$ increased by 0.72 nm after the adsorption of MFX reached its maximum capacity compared to an increase of 0.47 nm for CFX, 0.58 nm for OFX, and 0.5 nm for SFX. At pH 7, the increase was 0.72 nm for MFX compared to 0.37 nm for CFX, 0.44 nm for OFX, and 0.41 nm for SFX. It can also be noted that the increase in $d_{001}$ was similar for CFX, SFX, and OFX at both pH.

The XRD profiles of all adsorption isotherms are shown in Figures 22-26. At both pH, the shifting of the position $d_{001}$ shifts occurs as Q increases. The full-fixed width at half maximum intensity (fwhm) was reported along with Q and $d_{001}$ in Tables 3-4. The fwhm was minimum for pure MONT at both pH, but show no clear trend as adsorption increases.

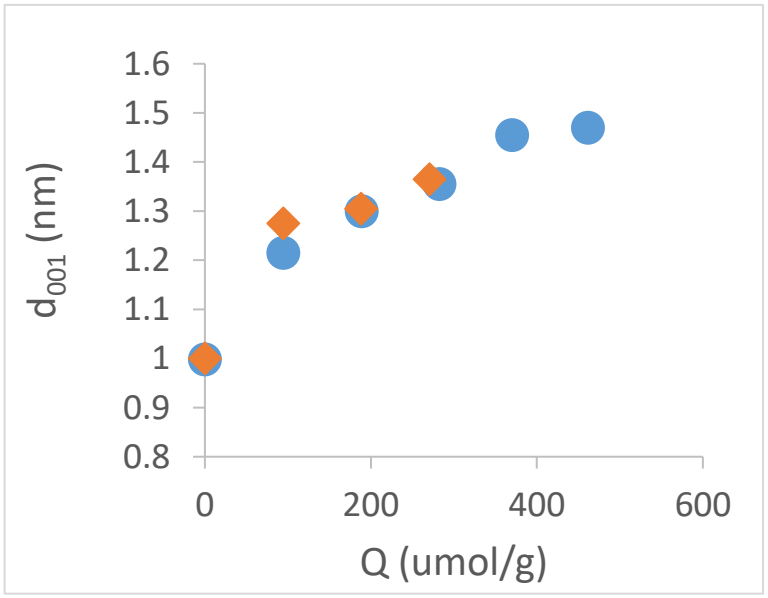


Figure 17. $d_{001}$ versus Q for CFX at pH 5 ( ) and pH 7 ( )

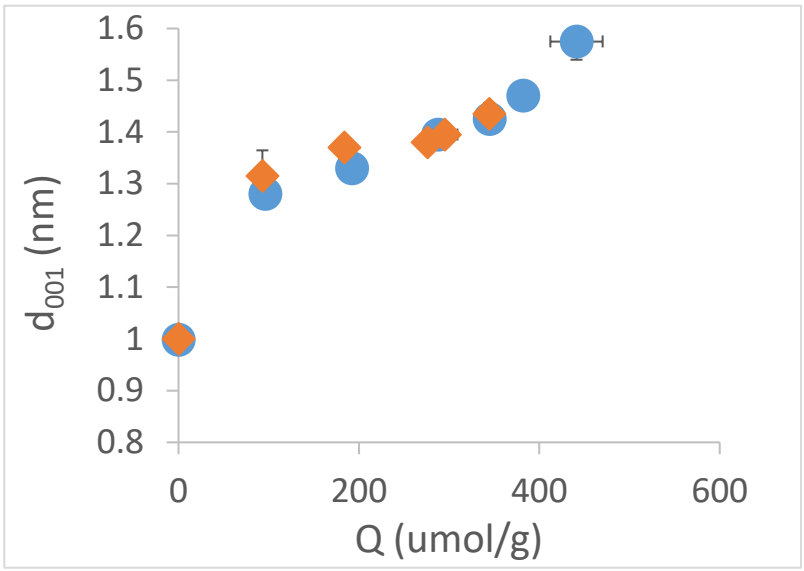


Figure 18. $d_{001}$ versus Q for OFX at pH 5 (●) and pH 7 (◆)

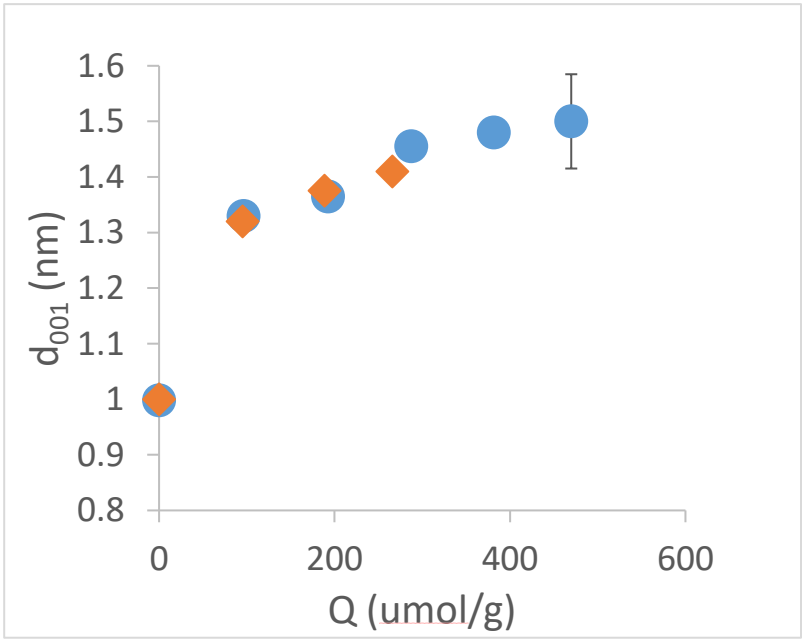


Figure 19. $d_{001}$ versus Q for SFX at pH 5 (●) and pH 7 (◆)

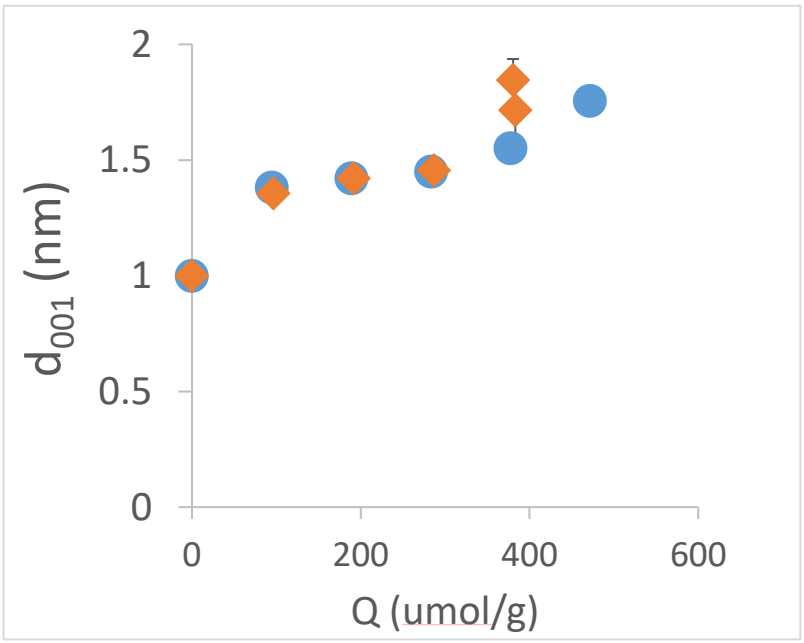


Figure 20. $d_{001}$ versus Q for MFX at pH 5 (●) and pH 7 (◆)

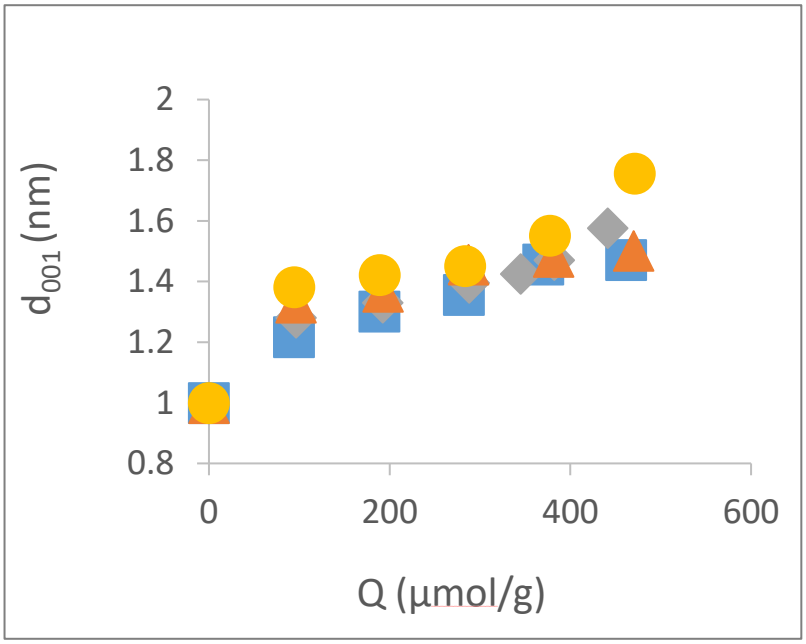


Figure 21. Interlayer spacing ($d_{001}$) vs adsorption values (Q) for CFX (■), OFX (◆), SFX (▲) and MFX (●) at pH 5

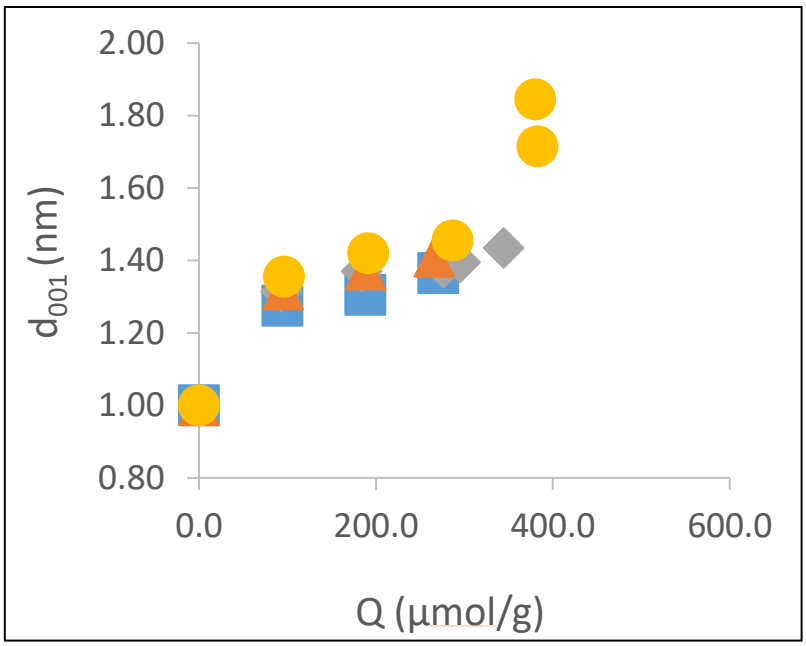


Figure 22. Interlayer spacing ($d_{001}$) vs adsorption values (Q) for CFX (■), OFX (◆), SFX (▲) and MFX (●) at pH 7

Table 3. Adsorption and X-ray diffraction results at pH 5

| CFX | | | | OFX | | | | SFX | | | | MFX | | | |
|---|---|---|---|---|---|---|---|---|---|---|---|---|---|---|---|
| Ci (uM) | Q (umol/g) | $D_{001}$ (nm) | Fwhm (2Θ) | Ci (uM) | Q (umol/g) | $D_{001}$ (nm) | Fwhm (2Θ) | Ci (uM) | Q (umol/g) | $D_{001}$ (nm) | Fwhm (2Θ) | Ci (uM) | Q (umol/g) | $D_{001}$ (nm) | Fwhm (2Θ) |
| 0 | 0 | 1 | 0.45 | 0 | 0 | 1 | 0.45 | 0 | 0 | 1 | 0.45 | 0 | 0 | 1 | 0.45 |
| 25 | 94.4 | 1.22 | 1.04 | 25 | 96.2 | 1.28 | 0.86 | 25 | 96.4 | 1.33 | 0.69 | 25 | 96.4 | 1.36 | 0.84 |
| 50 | 188.8 | 1.3 | 0.48 | 50 | 192.4 | 1.33 | 0.49 | 50 | 192.6 | 1.37 | 0.67 | 50 | 191.6 | 1.42 | 0.74 |
| 75 | 282.5 | 1.36 | 0.74 | 75 | 287.9 | 1.40 | 0.72 | 75 | 287.4 | 1.46 | 0.65 | 75 | 286.9 | 1.46 | 0.79 |
| 100 | 370.1 | 1.46 | 0.89 | 90 | 345 | 1.43 | 0.84 | 100 | 381.6 | 1.48 | 0.70 | 100 | 380.5 | 1.55 | 1.13 |
| 125 | 461.7 | 1.47 | 0.77 | 100 | 382.05 | 1.48 | 0.68 | 125 | 469.9 | 1.5 | 0.95 | 125 | 383.1 | 1.72 | 1.53 |
| | | | | 125 | 441.2 | 1.58 | 0.81 | | | | | | | | |

Table 4. Adsorption and X-ray diffraction results at pH 7

| CFX | | | | OFX | | | | SFX | | | | MFX | | | |
|---|---|---|---|---|---|---|---|---|---|---|---|---|---|---|---|
| Ci (uM) | Q (umol/g) | $D_{001}$ (nm) | Fwhm (2Θ) | Ci (uM) | Q (umol/g) | $D_{001}$ (nm) | Fwhm (2Θ) | Ci (uM) | Q (umol/g) | $D_{001}$ (nm) | Fwhm (2Θ) | Ci (uM) | Q (umol/g) | $D_{001}$ (nm) | Fwhm (2Θ) |
| 0 | 0.0 | 1.00 | 0.45 | 0 | 0.0 | 1.00 | 0.45 | 0 | 0.0 | 1.00 | 0.45 | 0 | 0.0 | 1.00 | 0.45 |
| 25 | 94.4 | 1.28 | 0.85 | 25 | 93.0 | 1.32 | 0.61 | 25 | 95.1 | 1.32 | 0.63 | 25 | 96.4 | 1.36 | 0.78 |
| 50 | 188.1 | 1.31 | 0.48 | 50 | 183.9 | 1.37 | 0.56 | 50 | 188.5 | 1.38 | 0.63 | 50 | 191.6 | 1.42 | 0.75 |
| 75 | 270.6 | 1.37 | 0.76 | 75 | 276.1 | 1.38 | 0.61 | 75 | 266.1 | 1.41 | 0.65 | 75 | 286.9 | 1.46 | 0.7 |
| | | | | 90 | 295.2 | 1.40 | 0.73 | | | | | 100 | 380.5 | 1.85 | 1.36 |
| | | | | 100 | 344.4 | 1.44 | 0.68 | | | | | 125 | 383.1 | 1.72 | 1.77 |

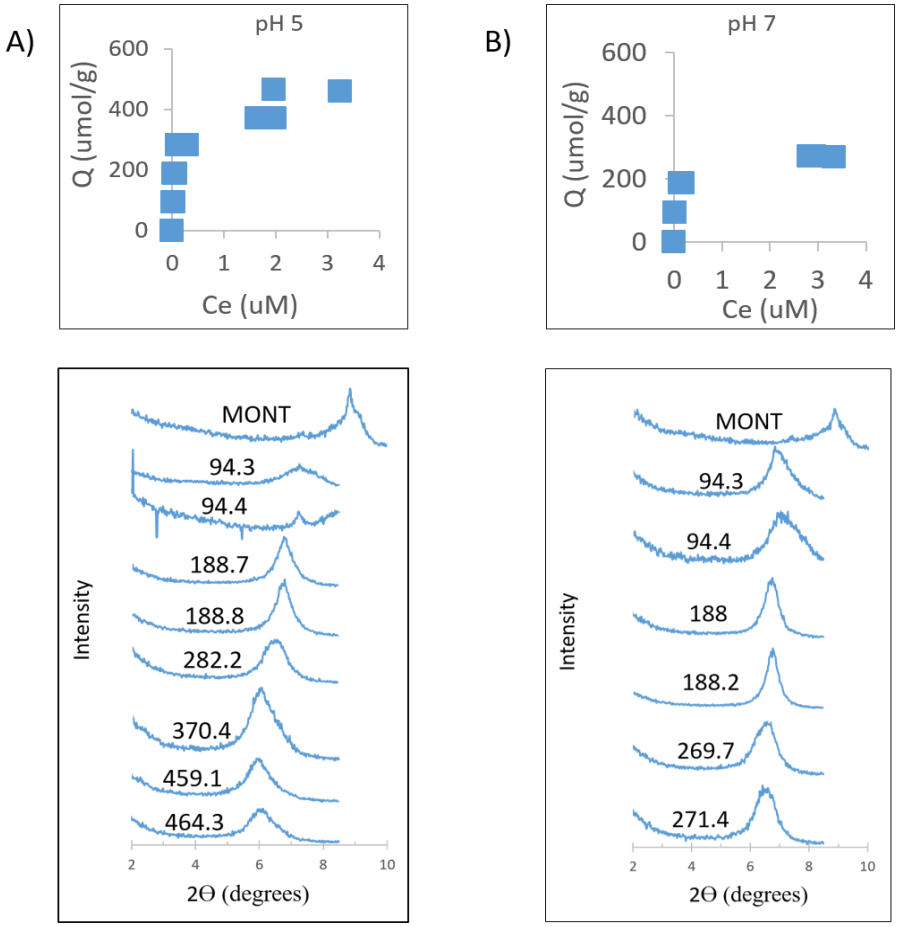


Figure 23. Amount of CFX adsorbed (Q, μmol $g^{-1}$) vs equilibrium concentration (Ce, μM) and associated XRD Profile. The numbers represent the Q values

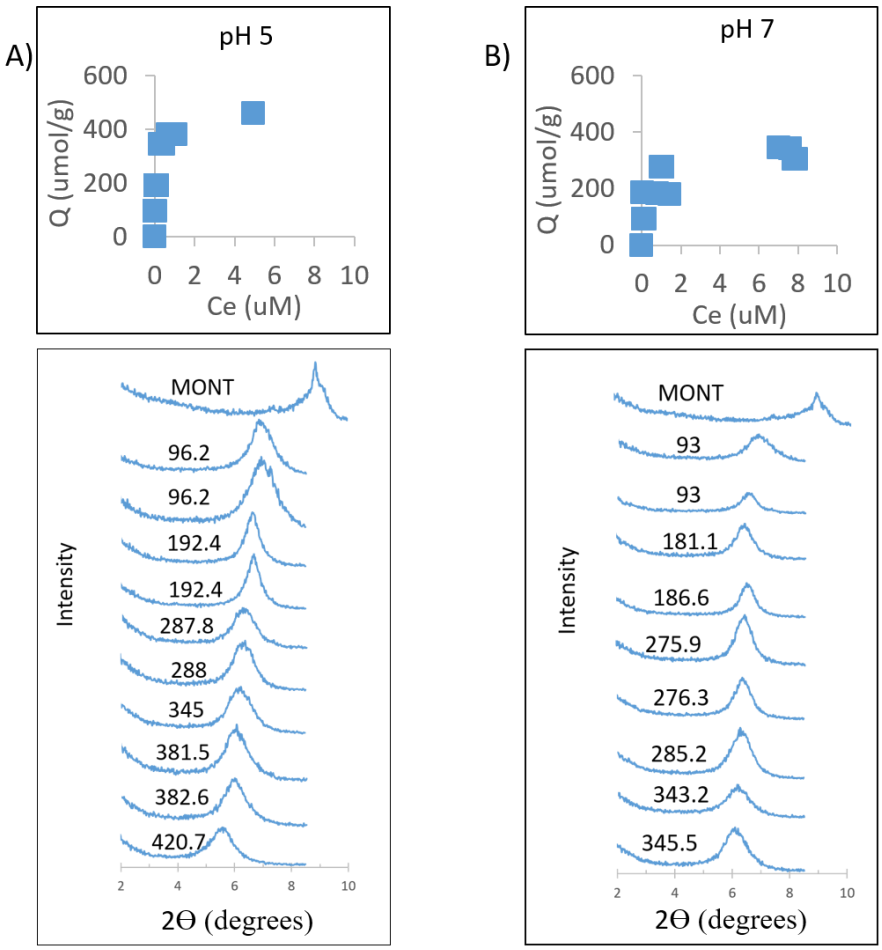


Figure 24. Amount of OFX adsorbed (Q, μmol $g^{-1}$) vs equilibrium concentration ($C_e$, μM) and associated XRD Profile. The numbers represent the Q values

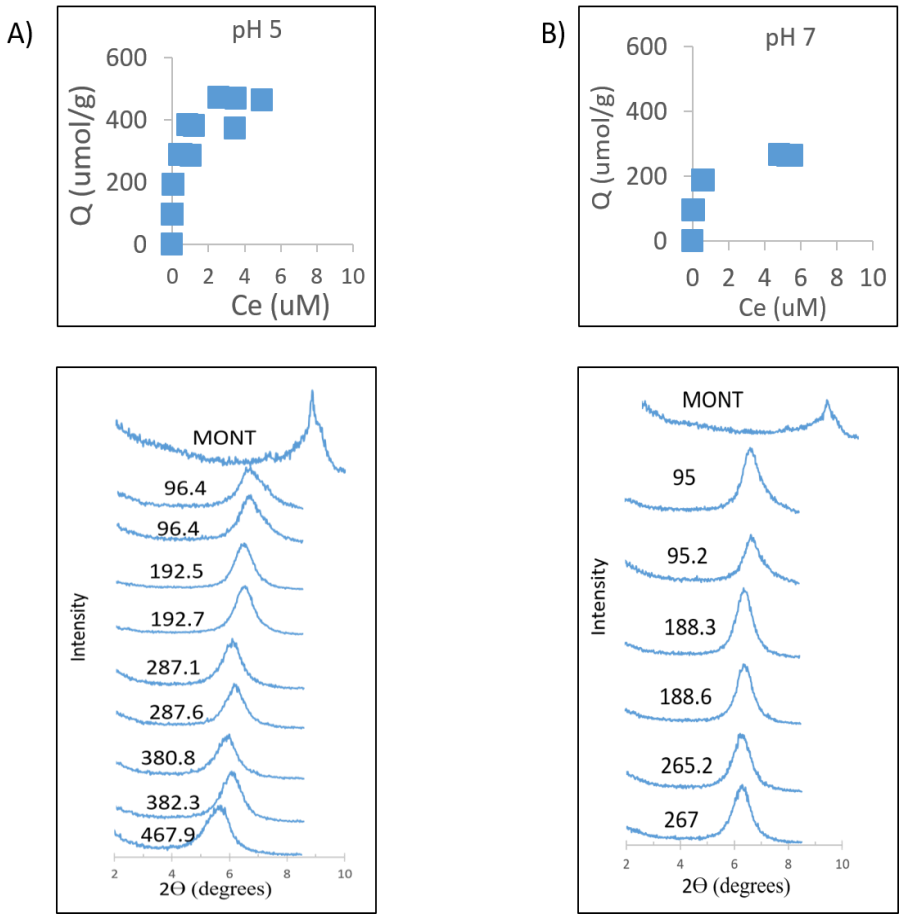


Figure 25. Amount of SFX adsorbed (Q, µmol $g^{-1}$) vs equilibrium concentration ($C_e$, µM) and associated XRD Profile. The numbers represent the Q values

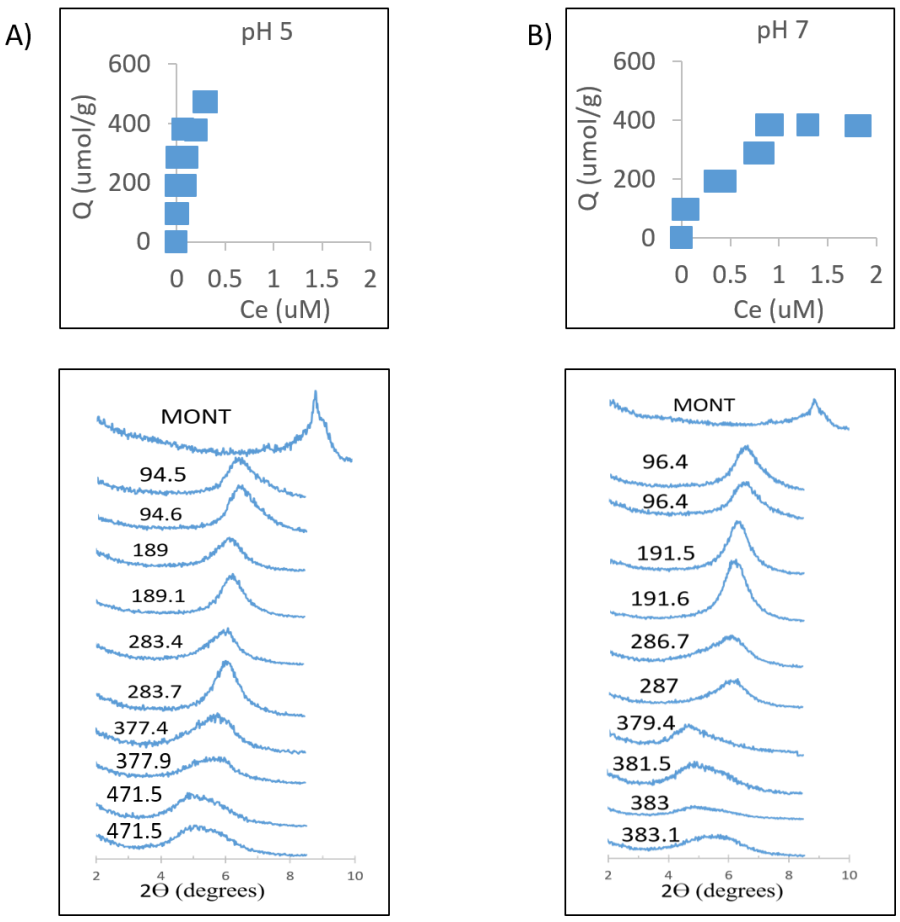


Figure 26. Amount of MFX adsorbed (Q, μmol $g^{-1}$) vs equilibrium concentration ($C_e$, μM) and associated XRD Profile. The numbers represent the Q values.

Monte Carlo Simulations

Figures 27-30 show the simulated adsorption of CFX, OFX, SFX, MFX on MONT at $d_{001}$ of 1.4, 1.6 and 1.8 nm. At these $d_{001}$, the FQs molecules have a planar conformation in the clay interlayer. The FQs adsorb onto the clay surface by either interacting directly with the surface or forming complexes with the $Na^+$ ions and water molecules. Three kinds of complexes formation can be noted in the figures below: FQ-$Na^+$-Clay, FQ-$Na^+$-Water-Clay, and FQ-Water-Clay. In the FQ-$Na^+$-Clay complex, the FQ molecule binds to the $Na^+$ ion, which then binds onto the clay

surface. In this case, the $Na^+$ ions are being stabilized by the FQ and the clay. In the FQ-$Na^+$-Water-Clay complex, the FQ molecule binds to the $Na^+$ ions, which bind to clay surface through hydrogen bonds with the water molecules. In other words, the FQ-$Na^+$ complexes are hydrated. In the FQ-Water-Clay complex, the FQ molecule binds to the clay surface through hydrogen bonds with the water molecules. This is known as water bridge. As $d_{001}$ increases, the FQ-$Na^+$-Water-Clay complexes were more dominant in the interlayer. At 1.4 nm, for all FQs, water bridges and the solvation of FQ-$Na^+$ complex occur at the carboxylic acid moiety. For CFX and MFX, the protonated amino group binds directly to clay surface whereas for OFX, it binds through a water bridge. For SFX, the piperazine group does not interact with the clay surface, however, the fluorine atom in the substituent $R_1$ (Figures 1 and 4) binds to the surface through a Water-$Na^+$ bridge. the FQ-$Na^+$ complexes bind to the surface indirectly through water molecules. At 1.6 nm, both the carboxylate group and the piperazine group bind to the surface through water bridges for all FQs. At 1.8 nm, both the carboxylate group and the piperazine group bind to the surface through water bridges for all FQs, at the exception of SFX. The fluorine atom at position $R_3$ (Figures 1 and 4) is involved in SFX interaction with the clay instead of the piperazine group. Hydration of the FQ-$Na^+$ complex is still present after intercalation of all four FQs.

Figures 2-5 show that the four FQs possess a keto group adjacent to the carboxylate group. This keto oxygen is often sharing a $Na^+$ ion with one of the carboxylate oxygens, as seen when $d_{001}$ = 1.4 nm in Figure 27-30, to stabilize the interactions with the surface.

Figure 30 C shows that at $d_{001}$ = 1.8 nm, MFX is enveloped by water molecules in the interlayer. Despite their planar conformation, CFX, OFX, and SFX are not as well enveloped in the interlayer as MFX. Figure 28 C shows that OFX starts to adopt a tilted conformation at 1.8 nm.

A B C

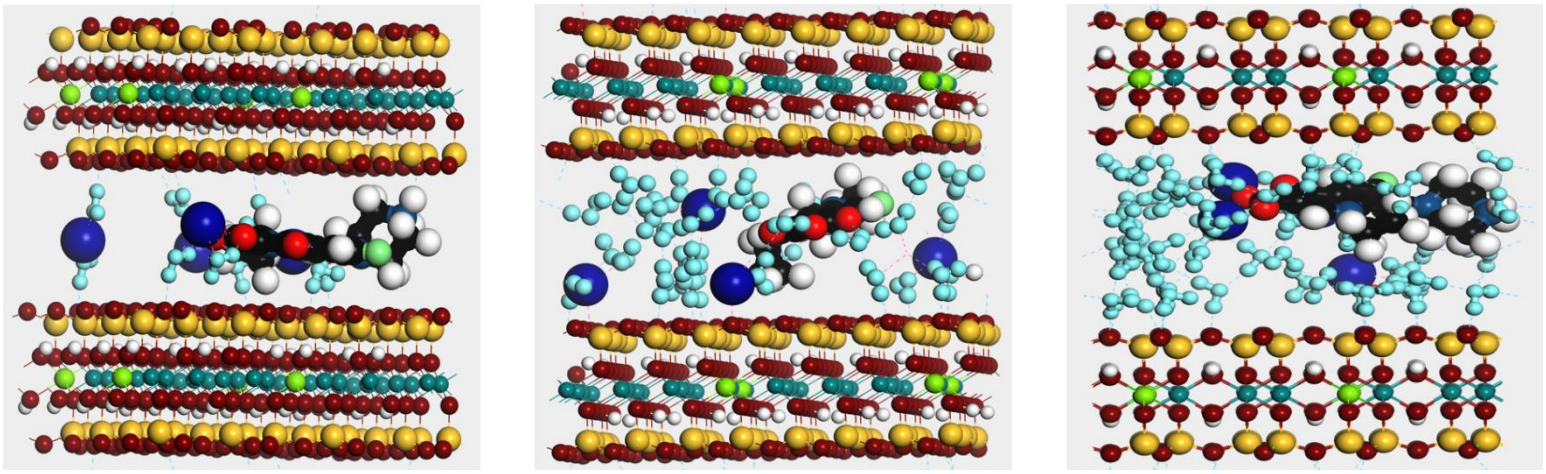

Figure 27. Monte Carlo Simulation of CFX on MONT at $d_{001}$ = 1.4 (A), 1.6 (B) and 1.8 nm (C)

A B C

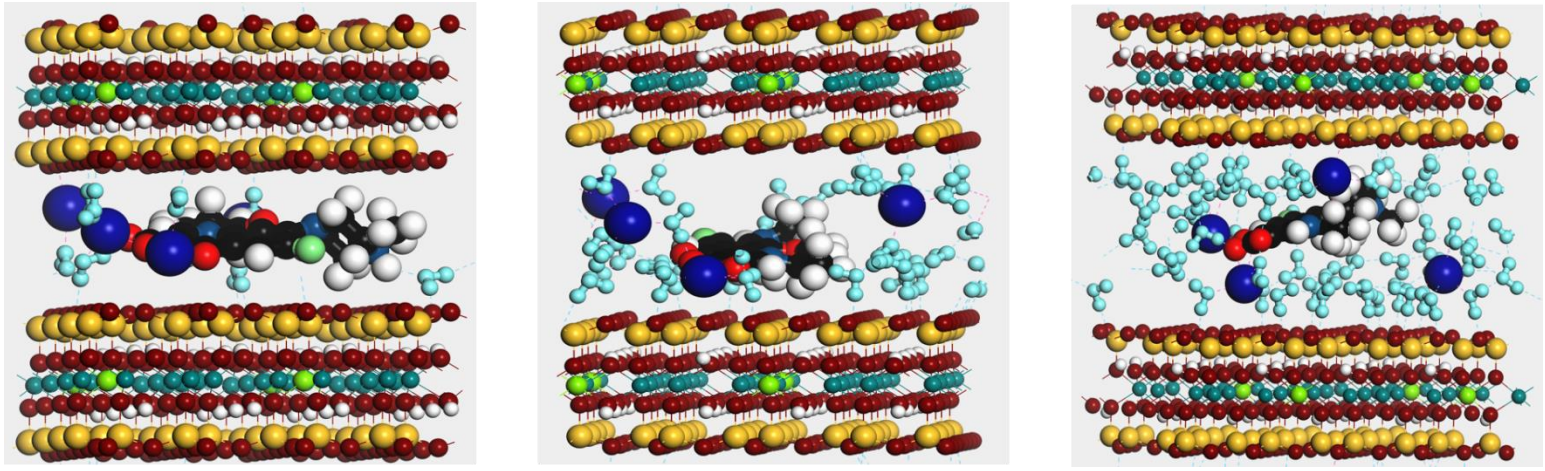

Figure 28. Monte Carlo Simulation of OFX on MONT at $d_{001}$ = 1.4 (A), 1.6 (B) and 1.8 nm (C)

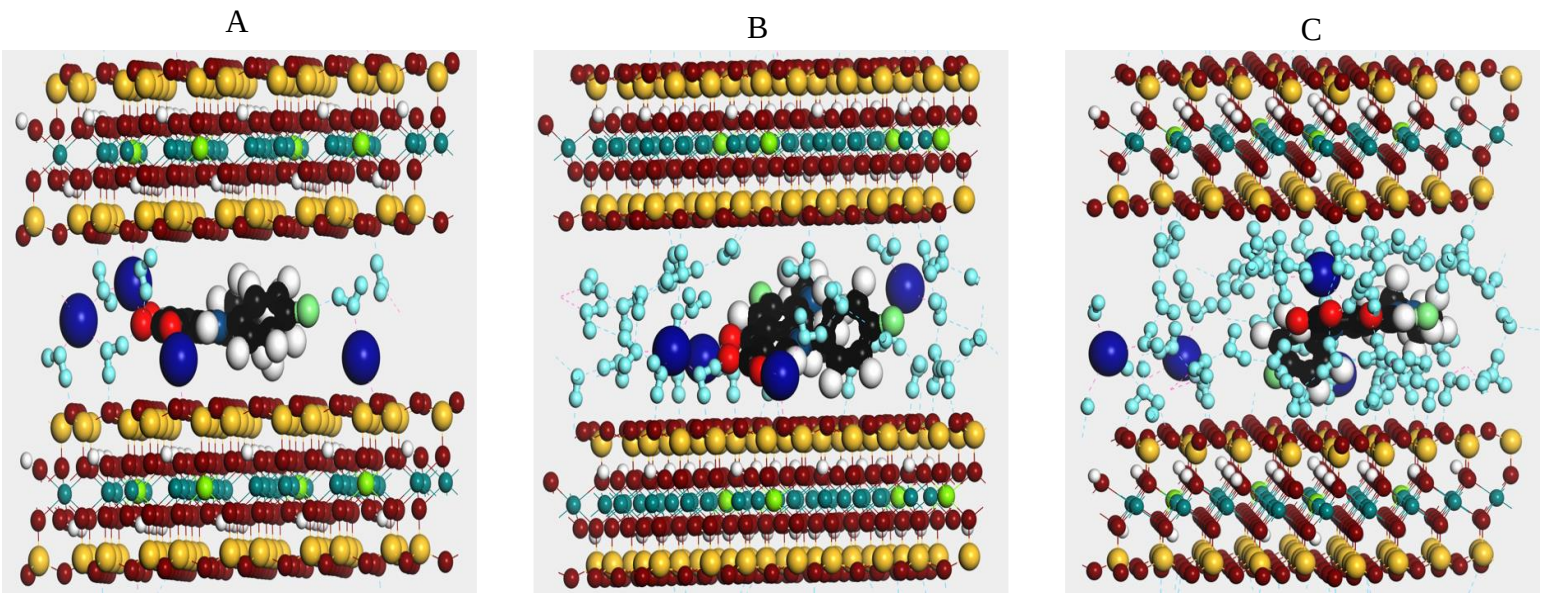


Figure 29. Monte Carlo Simulation of SFX on MONT at $d_{001}$ = 1.4 (A), 1.6 (B) and 1.8 nm (C)

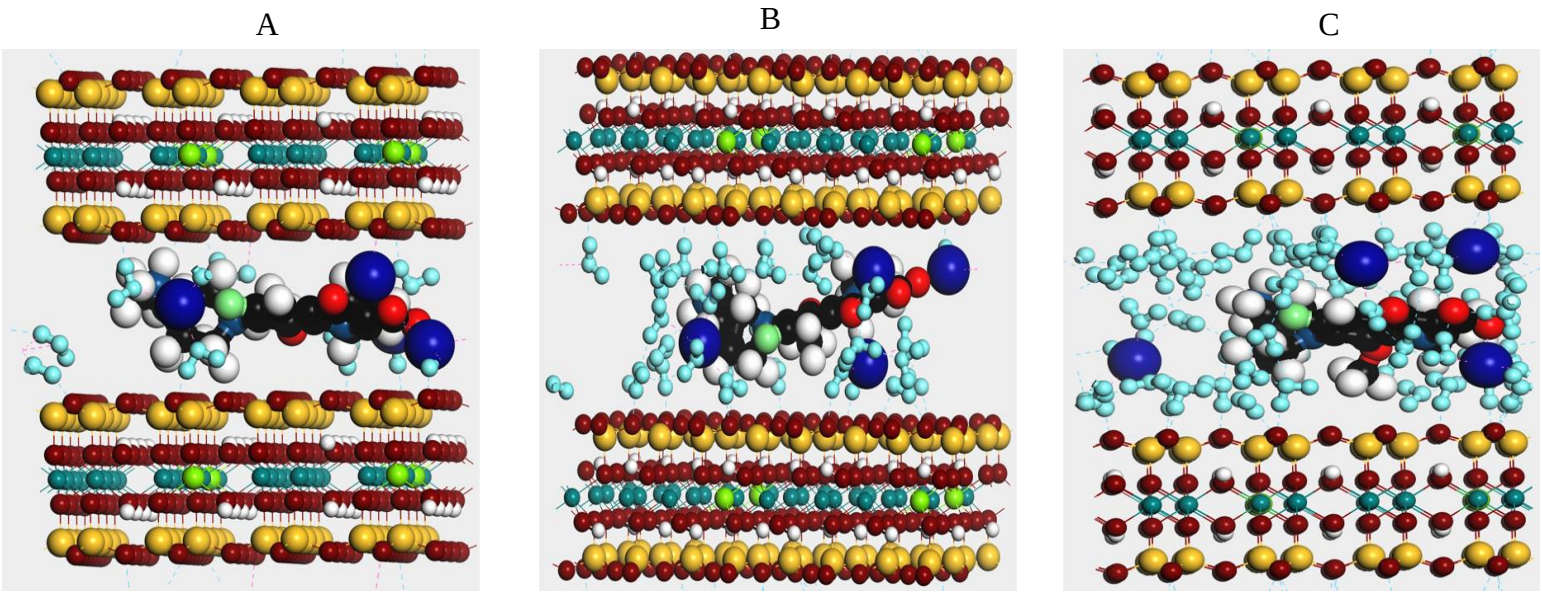


Figure 30. Monte Carlo Simulation of MFX on MONT at $d_{001}$ = 1.4 (A), 1.6 (B) and 1.8 nm (C)

**Discussion**

The results of the adsorption isotherms show higher adsorption of all four FQs at pH 5 than at pH 7 (Figures 11-16). As shown in Table 1, at pH 5, the FQs exist in their cationic form as a result of the protonation of the piperazine moiety, which may strongly bind to the negative

surface of the clay interlayer. This suggests that cation exchange reactions are promoted at pH 5. At pH 7, the FQs exist mostly as zwitterion (Table 2) where the protonated piperazine group and the deprotonated carboxylic acid group coexist. The protonated piperazine group would still bind to the surface of MONT, which facilitates the high adsorption of the FQs also at pH 7. At neutral and basic pH, the negatively charged carboxylate group of the FQs can participate in the adsorption mechanism by either forming complexes with cations or water molecules in the interlayer. These complexes then bind to the clay surface. We performed Monte Carlo adsorption simulations of the FQ zwitterions on montmorillonite. The results of our simulation agree with the hypothesis that hydration of FQ-metal complexes influences the trapping of FQs in 2:1 clay minerals put forward by Aristilde & Sposito [32]. As $d_{001}$ increases, the complexes formed by the FQ and $Na^+$ ions were increasingly hydrated by water molecules (Figures 27-30). Therefore, the retention of FQs in clay interlayer is also possible at neutral pH 7. Water molecules bridge interactions between the FQ compounds and the clay surface.

XRD analyses demonstrate that the adsorption behavior of the four FQs is different from their interlayer adsorption. For all FQs, the same $d_{001}$ was obtained at both pH 5 and 7 for the same Q implying that interlayer adsorption is independent of pH. However, for similar Q values, the adsorption of MFX resulted in a greater $d_{001}$ expansion at both pH implying different interstratification. Additionally, higher adsorption and lower equilibrium concentrations of MFX suggests that it has a higher affinity for MONT. Molecular modeling show that MFX adsorb differently in MONT interlayer (Figure 30 C).

## Conclusion

The results of this study show that pH and chemical structure play a determining factor in the adsorption of different generations of FQs. The influence of pH on FQ adsorption was similar for all four FQs of interest: a higher adsorption was observed at pH 5 than at pH 7. The $d_{001}$ obtained when adsorption reached its maximum values were not influenced by pH for all FQs. The differences in the adsorption of the four FQs were more noticeable at high equilibrium concentrations (greater than 0.1 μM) when the adsorption values of MFX and $d_{001}$ were higher than those of the other FQs. XRD and molecular modeling show reveal that MFX adsorbs differently.

**References**


1. Appelbaum P.C & Hunter P.A. The Fluoroquinolone Antibacterials: Past, Present and Future Perspectives. *International Journal of Antimicrobial Agents* 2000, 16:5-15
2. Andriole V.T. The Quinolones: Past, Present, and Future. *Clinical Infectious Diseases* 2005, 41:113-119
3. Siporin C. The Evolution of Fluorinated Quinolones: Pharmacology, Microbiological Activity, Clinical Uses and Toxicities. *Annual Review of Microbiology* 1989, 43:601-627
4. Chen G, Li M, Liu X. Fluoroquinolone Antibacterial Agent Contaminants in Soil/Groundwater: A Literature Review of Sources, Fate and Occurrence. *Water Air Soil Pollut*ion 2015, 226: 418
5. Goyne K.W, Chorover J, Kubicki J.D, Zimmerman A.R, Brantley S.L. Sorption of the antibiotic ofloxacin to mesoporous and nonporous alumina and silica. *Journal of Colloid and Interface Science* 2005, 283:160-170
6. Fatta-Kassinos D, Meric S, Nikolaou A. Pharmaceutical Residues in Environmental Waters and Wastewaters: Current State of Knowledge and Future Research. *Analytical and Bioanalytical Chemistry* 2011, 399(1):251-275
7. Golet E.M, Alder A.C, Giger W. Environmental Exposure and Risk Assessment of Fluoroquinolone Antibacterial Agents in Wastewater and River Water of the Glatt Valley Watershed, Switzerland. *Environment Science and Technology* 2002, 36(17):3645-3651
8. Kümmerer K. Antibiotics in the Aquatic Environment - a Review Part I. *Chemosphere* 2009, 75:417-434
9. Golet E.M, Strehler A, Alder A.C, Giger W. Determination of Fluoroquinolone Antibacterial Agents in Sewage Sludge and Sludge Treated Soils Using Accelerated

Solvent Extraction Followed by Solid Phase Extraction. *Analytical Chemistry* 2002, 74(21):5455-5462

10. Zhou L, Ying G, Zhao J, Wang L, Yang B, Liu S. Trends in the Occurrence of Human and Veterinary Antibiotics in the Sediments of the Yellow River, Hai River and Liao River in Northern China. *Environmental Pollution* 2011, 159:1877-1885
11. Kolpin D.W, Furlong E.T, Meyer M.T, Thurman E.M, Zaugg S.D, Barber L.B, Buxton H.T. Pharmaceuticals, Hormones, and Other Organic Wastewater Contaminants in US Streams, 1999-2000: A National Reconnaissance. *Environment Science & Technology* 2002, 36(6):1202-1211
12. Pico Y and Andreu V. Fluoroquinolones in Soils-Risks and Challenges. *Analytical and Bioanalytical Chemistry* 2007, 387:1287-1299
13. Wu Q, Li Z, Hong H. Adsorption of the quinolone antibiotic nalidixic acid onto montmorillonite and kaolinite. *Applied Clay Science* 2013, 74:66-73
14. Rivagli E, Pastorello A, Sturini M, Maraschi F, Speltini A, Zampori L, Setti M, Malavasi L, Antonella P. Clay Minerals for Adsorption of Veterinary Fluoroquinolones: Behavior and Modeling. *Journal of Environmental Chemical Engineering* 2014, 2:738-744
15. Jalil M.E, Baschini M, Sapag K. Influence of pH and antibiotic solubility on the removal of ciprofloxacin from aqueous media using montmorillonite. *Applied Clay Science* 2015, 114:69-76
16. Wang C, Li Z, Jiang W, Jean J, Liu C. Cation Exchange Interaction between Antibiotic Ciprofloxacin and Montmorillonite. *Journal of Hazardous Materials* 2010, 183:309-314
17. Yan W, Hu S, Jing C. Enrofloxacin Sorption on Smectite Clays: Effects of pH, cations and Humic Acid. *Journal of Colloid and Interface Science* 2012, 372:141-147

18. Aristilde L, Lanson B, Miehe-Brendle J, Marichal C, Charlet L. Enhanced Interlayer Trapping of a Tetracylcine Antibiotic Within Montmorillonite Layers in the Presence of Ca and Mg. *Journal of Colloid and Interface Science* 2016, 44:153-159
19. Wang C, Li Z, Jiang W. Adsorption of Ciprofloxacin on 2:1 Dioctahedral Clay. *Applied Clay Science* 2011, 53:723-728
20. Nowara A, Burhenne J, Spiteller M. 1997. Binding of Fluoroquinolone Carboxylic Acid Derivatives to Clay Minerals. *Journal of Agriculture and Food Chemistry* 45:1459-1463
21. Wu Q, Li Z, Hong H, Yin K, Tie L. Adsorption and Intercalation of Ciprofloxacin on Montmorillonite. *Applied Clay Science* 2010, 50:204-211
22. Wan M, Li Z, Hong H, Wu Q. Enrofloxacin Uptake and Retention on Different Types of Clays. *Journal of Asian Earth Sciences* 2013, 77:287-294
23. Carrasquillo A.J, Bruland A.A, MacKay D, Vasudevan D. Sorption of Ciprofloxacin and Oxytetracylcine Zwitterions to Soils and Soil Minerals: Influence of Compound Structure. *Environment Science & Technology* 2008, 42:7634-7642
24. Figueroa-Diva R.A, Vausdevan D, MacKay A.A. Trends in soil sorption coefficients within common antimicrobial families. *Chemosphere* 2010, 79:786-793
25. Alexy, R. and Kümmerer, K. Antibiotics for Human Use, in Organic Pollutants in the Water Cycle: Properties, Occurrence, Analysis and Environmental Relevance of Polar Compounds (eds T. Reemtsma and M. Jekel), Wiley-VCH Verlag GmbH & Co. KGaA, Weinheim, FRG, 2006. doi: 10.1002/352760877X.ch3
26. Lorenzo F, Navaratnam S, Edge R, Allen N.S. Primary Photophysical Properties of Moxifloxacin—A fluoroquinolone Antibiotic. *Photochemistry and Photobiology* 2008, 84:1118-11125

27. Aristide L & Sposito Garrison. Complexes of The Antimicrobial Ciprofloxacin with Soil, Peat and Aquatic Humic Substances. *Environmental Toxicology and Chemistry* 2013, 32(7):1467-1478

28. Accelrys Software Inc., 2013. Discovery Studio Modeling Environment. Accelrys Software Inc., San Diego

29. Pochodylo A.L, Aoki T.G, Aristilde L. Adsorption Mechanism of Microcystin Variants Conformations at Water-Mineral Interfaces: A Molecular Modeling Investigation. *Journal of Colloid and Interface Science* 2016, 480:166-174

30. Berendsen H.J.C, Grigera J.R, Straatsma T.P. The Missing Term in Effect Pair Potentials. *Journal of Physical Chemistry* 1987, 91:6269-6271

31. Cygan R.T, Liang J-J, Kalinichev A.G. Molecular Models of Hydroxide, Oxyhydroxide, and Clay Phases and the Development of a General Force Field. *Journal of Physical Chemistry B* 2004, 108(4):1255-1266

32. Aristilde L & Sposito G. Molecular Modeling of Metal Complexation by A Fluoroquinolone Antibiotic. *Environmental Toxicology and Chemistry* 2008, 27 (11):2304-2310